

# Explainable Unsupervised Change-point Detection via Graph Neural Networks

Ruohong Zhang <sup>\*1</sup> Yu Hao <sup>\*1</sup> Donghan Yu <sup>1</sup> Wei-Cheng Chang <sup>1</sup> Guokun Lai <sup>1</sup> Yiming Yang <sup>1</sup>

## Abstract

Change-point detection (CPD) aims at detecting the abrupt property changes lying behind time series data. The property changes in a multivariate time series often result from highly entangled reasons, ranging from independent changes of variables to correlation changes between variables. Learning to uncover the reasons behind the changes in an unsupervised setting is a new and challenging task. Previous CPD methods usually detect change-points by a divergence estimation of statistical features, without delving into the reasons behind the detected changes. In this paper, we propose a correlation-aware dynamics model which separately predicts the correlation change and independent change by incorporating graph neural networks into the encoder-decoder framework. Through experiments on synthetic and real-world datasets, we demonstrate the enhanced performance of our model on the CPD tasks as well as its ability to interpret the nature and degree of the predicted changes.

## 1. Introduction

Change-point detection (CPD) is an important component in understanding the complex dynamics of sequential data. Detecting changes in multivariate time series can be more challenging than in univariate time series, because when multiple variables interact with each other, and the reasons behind the change-points are often complicated.

Learning to uncover the reasons behind a change-point is useful in real-life applications. For example, traders perform pair trading to profit from the correlated stocks in the market, such as Apple and Samsung, which share similar dips and highs. News about Apple opening market in other countries may independently raise its price without breaking its correlation with Samsung. However, news about Apple building

<sup>\*</sup>Equal contribution <sup>1</sup>Carnegie Mellon University. Correspondence to: Ruohong Zhang <[ruohongz@cs.cmu.edu](mailto:ruohongz@cs.cmu.edu)>, Yu Hao <[yuahao2@cs.cmu.edu](mailto:yuahao2@cs.cmu.edu)>.

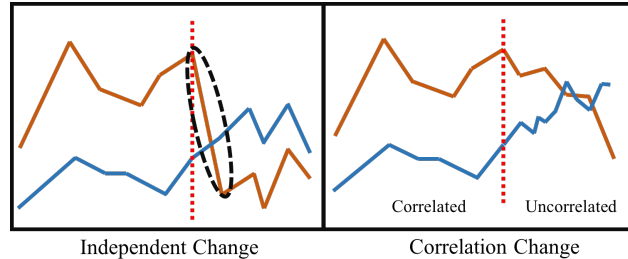


Figure 1. The left figure is an independent change of a variable, and the right figure is a correlation change between the two variable. Detecting the two types of change in unsupervised setting is a challenging task for CPD

self-driving cars will break its correlation with Samsung, and establish new correlations with automobile companies. Both news causes change-points on stock prices, but the first type is an **independent change** of variables, while the second type is a **correlation change** between variables.

A learning model that distinguishes the two kinds of changes can bring enhanced interpretability, and assist humans to understand the *nature* and *degree* of the changes that happened in multivariate time series. Unfortunately, previous statistical or neural network CPD models largely neglect this task of separating correlation change from independent change.

Most statistical CPD models are based on either statistical inference, i.e. Bayesian CPD (Barry & Hartigan, 1993; Xuan & Murphy, 2007), BOCPD (Adams & MacKay, 2007; Garnett et al., 2010; Saatçi et al., 2010), or hypothesis tests including two-sample MMD kernel methods (Gretton et al., 2012; Li et al., 2015), CUMSUM ratio test (Gombay et al., 1996), or density-ratio estimation (Liu et al., 2013). Recently, deep neural models provide powerful tools to estimate the time-series distribution. Although better performances were achieved, neural models usually serve as better kernel functions (Chang et al., 2019), or density ratio estimators (Khan et al., 2019). The purpose of these models is to detect changes, but not to reason for the cause of changes.

In order to separate the two types of changes, a learning

method has to capture the dynamics of the correlation behind multivariate time series. Previous work focused on implicit interaction model (Sukhbaatar et al., 2016; Guttenberg et al., 2016), which uses message passing or attention mechanism for latent relation representation, or explicitly interaction model (Kipf et al., 2018; Li et al.), which infers interaction using graph-based auto-encoder from observed data. However, those models assume that the underlying relationship is static, and don't capture the change of correlation over time.

In this work, we propose a Correlation-aware Dynamics Model for Change-point Detection (CORD-CPD), which is an encoder-decoder architecture that separately predicts change-point scores of two types: correlation changes and independent changes. The correlation changes are measured by the encoder which uses graph neural networks to extract the correlations between variables in observed time series, and the independent changes are determined by the decoder which learns the systematical dynamics of variables. Our contributions are as follows:

- We tackle the challenging problem of explainable change-point detection in multivariate time series involving two types of changes: correlation changes and independent changes.
- We propose a novel framework CORD-CPD that separately predicts the two types of changes, and ensembles them for robust change-point detection.
- Experiment on synthetic and real datasets demonstrates that our model brings interpretability and enhanced performance and in CPD tasks.

## 2. Problem Definition

In this work, we study CPD problem in the multivariate time series setting. We assume that the time series could be generated by hidden parameters. The exact parameters are generally unknown, but we assume they can control the dynamics of the individual variable, as well as the correlation between them.

Formally, the set of time series data we observe is  $\{\mathbf{X}_i\}$ , where each  $\mathbf{X}_i$  is a series of observations  $\{\mathbf{x}^1, \mathbf{x}^2, \dots, \mathbf{x}^T\}$ . The time series involves  $N$  variables with  $M$  features for each, such that  $\mathbf{x}^t \in \mathbb{R}^{N \times M}$ . We denote by  $\mathbf{x}_i^t$  the feature vector of variable  $i$  at time  $t$ . Features are helpful to determine the dynamics of variables; however in real-world scenario, not all dataset has additional features (such that  $M = 1$ ). In this case, we use ‘subsequence’ as the feature vector,  $\mathbf{x}_i^t = [x_i^t, x_i^{t+1}, \dots, x_i^{t+K-1}]$  for some  $K > 1$ .  $\mathbf{X}_i \in \mathbb{R}^{T \times N \times K}$  is also known as Hannkel matrix (Liu et al., 2013), which plays an important role in multivariate CPD (Kawahara et al., 2007; Moskvina & Zhigljavsky, 2001).

Change-point happens in a time series when there is an abrupt change of property, and our goal is to detect the change in a retrospective and unsupervised setting. Formally, if  $\{\mathbf{X}_i\}$  has a change-point at time step  $t$ , it satisfies:

$$\begin{aligned} \{\mathbf{x}^1, \mathbf{x}^2, \dots, \mathbf{x}^{t-1}\} &\sim \mathbb{P}(\mathbf{x}) \\ \{\mathbf{x}^t, \mathbf{x}^{t+1}, \dots, \mathbf{x}^T\} &\sim \mathbb{Q}(\mathbf{x}) \end{aligned}$$

For some  $\mathbb{P}$  and  $\mathbb{Q}$  unknown. The difference between  $\mathbb{P}$  and  $\mathbb{Q}$  could be from two types of reasons: correlation change and independent change.

Building interpretable model for CPD is a challenging task. We will introduce our methodology in Section 3. In the Section 4, we will describe our model architecture and in Section 5 6, we show our experimental results and analysis.

## 3. Method

In this section, we will explain our method to track correlation changes and independent changes in a multivariate time series, and propose our solution to learn to detect them in an unsupervised way. Our CORD-CPD model separately predicts the scores both types of changes and ensemble them for a final prediction.

### 3.1. Correlation-aware Dynamic Model

To account for the type of change-points, we consider two kinds of hidden variables guiding the values of time series. The first type, hidden variables for *dynamics*, arises from the inherent property of the system, e.g. physical laws, market supply & demand. Dynamics is the law of motion of independent variables. The second type, hidden variables for *correlation*, corresponds to the interaction between the variables, e.g. particle attraction, company cooperation. Correlations take effects when variables operate together and interact.

Our CORD-CPD model is a correlation-aware dynamic model that will separate the effect of correlation and dynamic from observed data. The encoder extracts the correlation from variables, and the decoder captures the dynamics rule from the values of time series.

### 3.2. Correlation Change

In order to detect changes of correlation, the encoder of CORD-CPD extracts an affinity matrix of variables at each time step,  $\{\mathbf{A}^1, \mathbf{A}^2, \dots, \mathbf{A}^T\}$  where  $\mathbf{A}^t \in \mathbb{R}^{N \times N}$ . Each cell in  $\mathbf{A}^t$  is between 0 and 1, indicating how much they are related. The score of correlation change  $s_r$  is calculated by the  $L_1$  distance between two neighbor predicted relations:

$$s_r^t = \|\mathbf{A}^t - \mathbf{A}^{t-1}\|, t \geq 1$$

### 3.3. Independent Change

Given the correlation as input, the decoder estimates the expected value of time series under the learnt dynamics rule. In a short period of time, if a system follows the dynamics rule, the expected value will be close to the observed value; If a system has an abrupt independent change occurred, those values will be different. In experiments, we set the period to be  $k = 5$  steps. The independent change-point score  $s_d$  is calculated by the distance of the expected value  $\hat{\mathbf{w}}^t = \{\hat{\mathbf{x}}^{t+1}, \hat{\mathbf{x}}^{t+2}, \dots, \hat{\mathbf{x}}^{t+k}\}$  and the observed value  $\mathbf{w}^t = \{\mathbf{x}^{t+1}, \mathbf{x}^{t+2}, \dots, \mathbf{x}^{t+k}\}$ :

$$s_{d(t)} = \text{Dist}(\hat{\mathbf{w}}^{t-1}, \mathbf{w}^{t-1}), t \geq 1$$

where we use MSE as our choice for Dist function.

### 3.4. Ensemble of Changes

The encoder and decoder separately predict the scores for correlation changes and independent changes. A change-point occurred in a multivariate time series could result from one of them, or a mixture of both. In this study, we provide a simple way to ensemble the scores that yields good performance in practice. The ensemble score  $\mathbf{s}_{en}$  is calculated by:

$$\mathbf{s}_{en} = \text{Norm}(\mathbf{s}_r) + \text{Norm}(\mathbf{s}_d)$$

$$\text{Norm}(\mathbf{s}) = \frac{\mathbf{s} - u_s}{\sigma_s}$$

where  $u_s$  and  $\sigma_s$  are mean and standard deviation of  $\mathbf{s}$ .

## 4. Model Architecture

In this section, we describe our CORD-CPD architecture which has an encoder for correlation extraction and decoder for dynamical model.

We denote the time series from time  $t_1$  to  $t_2$  inclusively as  $\mathbf{X}^{[t_1, t_2]}$ . The encoder outputs a relation matrix  $\mathbf{A}^t$  for each time step  $t$ , as defined in 3.2. In our retrospective setting, we provide the entire time-series as input.

$$\text{enc}_\phi(\mathbf{A}|\mathbf{X}) = \prod_{t=1}^T \text{enc}_\phi(\mathbf{A}^t|\mathbf{X}^{[1, t]}) \quad (1)$$

The decoder reconstructs the time series by recovering the value  $\mathbf{x}^{t+1}$  auto-regressively with  $\mathbf{A}^t$  and  $\mathbf{X}^{[1, t]}$ .

$$\text{dec}_\theta(\mathbf{X}^{[2, T]}|\mathbf{A}) = \prod_{t=1}^T \text{dec}_\theta(\mathbf{x}^{t+1}|\mathbf{X}^{[1, t]}, \mathbf{A}^t) \quad (2)$$

The objective function of our autoencoder is:

$$\mathcal{L} = \mathbb{E}_{\text{enc}_\phi(\mathbf{A}|\mathbf{X})} [\log \text{dec}_\theta(\mathbf{X}|\mathbf{A})] \quad (3)$$

### 4.1. Correlation Encoder

As shown in Figure 2, the goal of the encoder is to calculate a correlation matrix  $\mathbf{A}^t$  at each timestep  $t$ , given the entire time-series  $\mathbf{X} \in \mathbb{R}^{T \times N \times M}$ , where  $T$  is the number of time-steps,  $N$  is the number of variables and  $M$  is the number of features. We propose a temporal encoding layer (TE) to capture both temporal dependencies between  $T$  steps and a spatial encoding layer (SE) to model the interaction between  $N$  variables. Specifically, we alternatively apply the TE and SE modules to progressively incorporate the temporal feature and the correlation feature into the latent embeddings of each variable. Finally, we predict the relation between every pair of variables by a 1-layer fully-connected network using the concatenation of the embeddings between them. Mathematically, for any two variables  $i$  and  $j$ , the relation is calculated by:

$$\mathbf{Y} = \text{TE}_2(\text{SE}(\text{TE}_1(\mathbf{X}))) \quad (4)$$

$$\mathbf{A}_{i,j}^t = \text{Softmax}(\text{FC}([\mathbf{Y}[t, i, :]; \mathbf{Y}[t, j, :]])) \quad (5)$$

The equation 4 and 5 shows the structure of our encoder.

In implementation,  $\mathbf{Y} \in \mathbb{R}^{T \times N \times H}$  has the same first two dimensions  $T$  and  $N$  as  $\mathbf{X}$ , because both the spatial and temporal encoding layer will preserve the number of time-steps and variables. If we want to capture multiple relations in a time series, each  $\mathbf{A}_{i,j}^t$  could be a high dimensional vector representing the probability distribution on different types of edge. We apply Gumbel-Softmax (Jang et al., 2017) to enforce sparse connections in the graphs and to reduce noise.

In the next sub-sections, we describe in details of our design of the TE and SE layers.

#### 4.1.1. TEMPORAL ENCODING LAYER

It is hard to detect the influence of the relation between variables by only observing a single time-step. Inferring the relation from a series of observations would be easier, because the difference between observations from different time-steps is usually informative. The TE layer captures both the long- and short-term dependencies. Take  $\mathbf{X} \in \mathbb{R}^{T \times N \times M}$  as input, the TE layer will encode each of the  $N$  variables separately and identically. In other words, we feed  $N$  representations  $\mathbf{X}[:, i, :] \in \mathbb{R}^{T \times M}$  into the TE layer in parallel, where  $i = 1, 2, \dots, N$ . We propose two types of temporal encoding layer: the  $\text{RNN}_{\text{TE}}$  and the  $\text{Trans}_{\text{TE}}$ .

**RNN<sub>TE</sub>** The recurrent neural networks are good at capturing temporal dependencies. Therefore, we use a bidirectional GRU network(Cho et al., 2014) as the RNN-based temporal encoder. We noticed that the bidirectional GRU, which captures both forward and backward time steps,

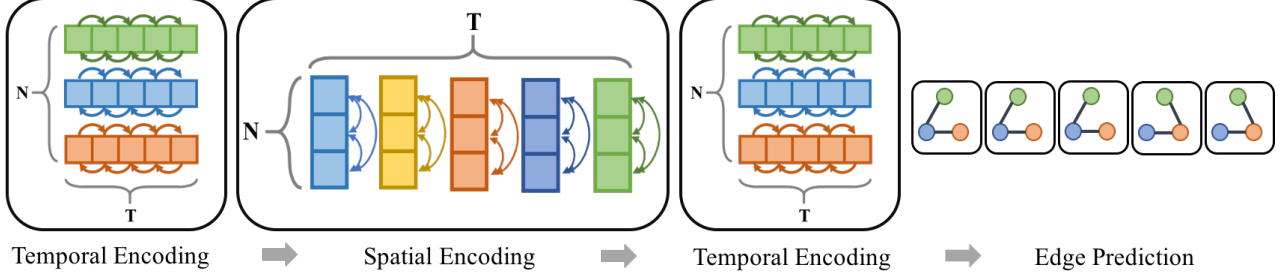


Figure 2. CORD-CPD Encoder: the encoder extracts correlation changes from multivariate time series, and outputs an affinity matrix at each step. The temporal encoding network captures time dependent features, and the spatial encoding network models relational features between variables.

is empirically superior than unidirectional GRU. It indicates retrospective change-point detection gives more reliable predictions than the online change-point detection in our task. The following equations shows the encoded representation of the  $i^{\text{th}}$  variable at the  $t^{\text{th}}$  step is computed by concatenating the output from the two directions of GRU.

$$\vec{h}_i^t = \overrightarrow{\text{GRU}}(\vec{h}_i^{t-1}, \mathbf{X}[t, i, :]) \quad (6)$$

$$\overleftarrow{h}_i^t = \overleftarrow{\text{GRU}}(\overleftarrow{h}_i^{t+1}, \mathbf{X}[t, i, :]) \quad (7)$$

$$\mathbf{h}_i^t = [\vec{h}_i^t, \overleftarrow{h}_i^t] \quad (8)$$

**TransTE** Although GRU is designed to combat the gradient vanishing problem, it still requires a long propagation path to capture long-range dependencies. A good alternative to solve the problem is by the Transformer model (Vaswani et al., 2017), which uses a self-attention mechanism to aggregate information between any two embeddings. In this way, Transformer can be useful to capture both long- and short-term dependents. Both of the dependencies are crucial to our task, because local dynamics are reflected by short period of time, and correlations are revealed in a long time duration.

Similar to (Vaswani et al., 2017), we use a positional encoding to incorporate the position information for TE. Then the embeddings are processed by a block consists of a multi-head self-attention layer and a feed-forward network, and each of them is followed by residual connection and layer normalization.

#### 4.1.2. SPATIAL ENCODING LAYER

The TE layers itself may not be able to model the correlation between variables through time. To inject an inductive bias for relation learning, we use graph neural networks (GNN) (Kipf & Welling, 2016) to learn the correlation. The purpose of SE is to integrate the information among all variables at each time-step. As shown in Figure 2, the SE layer is

orthogonal to the TE layer. We propose the following two types of modules: GNN<sub>SE</sub> and TransSE.

**GNN<sub>SE</sub>** Similar to (Kipf et al., 2018), we use the a message passing mechanism of GNN to aggregate information from neighbor nodes. The following equations show how the messages are passed in one layer of our GNN<sub>SE</sub>:

$$\tilde{\mathbf{h}}_{i,j} = f_e([\mathbf{x}_i; \mathbf{x}_j]) \quad (9)$$

$$\mathbf{h}_j = f_v(\mathbf{x}_j + \sum_{i \neq j} \tilde{\mathbf{h}}_{i,j}) \quad (10)$$

Both  $f_e(\cdot)$  and  $f_v(\cdot)$  are MLPs. The  $[\cdot]$  represents the concatenation of vectors.

Graph-based models gather neighborhood information by an aggregation and combination process (Xu et al., 2018). Equation 9 aggregates the neighborhood information and equation 10 combines the neighboring features by a summation. Graph networks are especially good at learning relations by sharing information from local to global. The learning complexity will be significantly decreased, compared to a fully-connected MLP (Xu et al., 2019).

**TransSE** Transformer can also be considered as a graph-based model which operates on a fully-connected graph (Kool et al., 2018), since the pairwise multi-head attention aggregates information from neighboring nodes. Compared to GNN, Transformer has additional well-designed structure of residual connection and layer normalization, which could be an advantage of TransSE for spatial encoding. Similar to GCN<sub>SE</sub>, Transformer enables message exchanging among the multiple variables. However, the positional encoding layer is removed, because variables are order invariant.

#### 4.2. DYNAMICS DECODER

The decoder module learns the dynamics rule of a system, and recovers the expected value of time series. As shown in Figure 3, the decoder calculates the expected dynamics

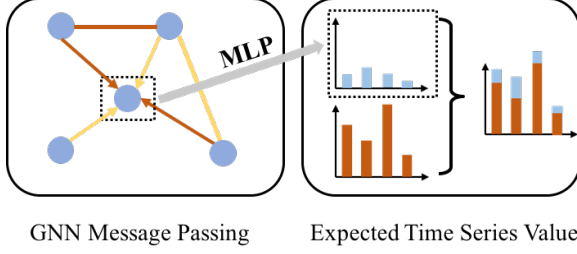


Figure 3. CORD-CPD decoder: Given the correlation graph, the decoder recovers the expected value of time series from learnt dynamics.

change at each time step, by  $\text{dec}_\theta(\mathbf{x}^{t+1} | \mathbf{X}^{[1,t]}, \mathbf{A}^t)$ . Since the dynamics are guided by the correlation, we also use a graph-based model to incorporate relational information into embeddings. For each relation type  $k$ , we have a distinct function  $g_e^k(\cdot)$  for the message passing. The functions  $g_e^k(\cdot)$  and  $g_v(\cdot)$  MLPs.

$$\mathbf{c}_{i,j}^t = \sum_k \mathbf{A}_{i,j}^t g_e^k([\mathbf{x}_i^t, \mathbf{x}_j^t]) \quad (11)$$

$$\mathbf{c}_j^t = g_v(\mathbf{x}_j + \sum_{i \neq j} \mathbf{c}_{i,j}^t) \quad (12)$$

$\mathbf{A}_{i,j,k}^t \in [0, 1]$  represents the probability of the  $k^{\text{th}}$  relation type. If the relation type vector  $\mathbf{A}_{i,j}^t$  is one-hot, only one type of relation will be active. If  $\mathbf{A}_{i,j}^t$  is a soft-max probability vector, it would calculate a distributed sum of the messages propagated through different types of relations.

Reconstructing time series performed by calculating the dynamic change with the help of MLP or RNN ( $g_{\text{out}}$ ). MLP work be a simle choice if the feature vector of a variable is good enough to predict the dynamics; otherwise RNN is preferable to aggregate history information from time series. Together we have:

$$\boldsymbol{\mu}_j^{t+1} = \mathbf{x}_j^t + \Delta \mathbf{x}_j^t = \mathbf{x}_j^t + g_{\text{out}}(\mathbf{c}_j^t) \quad (13)$$

$$\text{dec}_\theta(\mathbf{x}^{t+1} | \mathbf{X}^{[1,t]}, \mathbf{A}^t) = \mathcal{N}(\boldsymbol{\mu}^{t+1}, \sigma^2 \mathbf{I}) \quad (14)$$

Then we can minimize the reconstruction error:

$$\mathcal{L}_{\text{rec}} = \sum_j \sum_{t=2}^T \frac{\|\mathbf{x}_j^t - \boldsymbol{\mu}_j^t\|^2}{2\sigma^2} \quad (15)$$

### 4.3. Relation Smoothness Regularization

Since change-points are sparse in time series, we don't expect sharp changes to occur too frequently between the encoded relations. We add an additional regularization loss to control the smoothness of relation and to prevent instability:

$$\mathcal{L}_{\text{smooth}} = \frac{1}{T-1} \sum_{t=2}^T \|\mathbf{A}^t - \mathbf{A}^{t-1}\|_2^2 \quad (16)$$

The final loss function is:

$$\mathcal{L} = \mathcal{L}_{\text{rec}} + \lambda \mathcal{L}_{\text{smooth}} \quad (17)$$

where  $\lambda$  controls the relative strength of smoothness regularization.

## 5. Experiment with Physical Simulation

In this section, we describe the experiment setting including (1) synthesize different types of change-point appeared in the physical movement of particle-spring (2) evaluation metric (3) result analysis.

### 5.1. Particle-spring Change-point Simulation

We use a simulated system of particles connected by springs, similar to (Kipf et al., 2018). The dataset is generated by simple physical rules like Newton's law, Hooke's law, and Markov property. The particles moves in a 2D grid are connected by unobserved springs. We use 5 particles to generate a set multivariate time series of length 100, including a change-point that uniformly sampled from range [25, 75]. The features of each particle is 4 dimensions, including its location and speed:  $l_x, l_y, v_x, v_y$ .

In our system, trajectories are generated by 3 latent factors: initial location  $l$ , initial speed  $v$  and spring connection  $r$ . Based on the nature of factors, we generate 3 types of change points by perturbing location, speed, and connections at the change-point:

1. **location:** Add a perturbation to the current location by a Gaussian noise  $N(0, 0.1)$ , where the range of location is  $[-5, 5]$ .
2. **speed:** Add a perturbation to the current speed by a Gaussian noise  $N(0, 0.02)$ , and where range of speed is  $[-1, 1]$ .
3. **connection:** re-sample a new relation to make sure at least 5 pairs out of 10 are changed.

The change of location or speed belongs to the independent change of variables, since they only affect the feature of variables independently, and the change of connection belongs to a correlation change of variables. We realize that the perturbation added to the feature is relatively small, and this greatly increases the difficulty for a CPD task.

The synthetic dataset is helpful in two ways. First, the change-point is from either a correlation change or a independent change, and it can test the ability of a model to separate them. Second, it is also interesting to evaluate other on baselines to test which types of change-point they are good at.

## 5.2. Training and Testing

We generate 500 time series for each type of change and mix them together as training data, totally 1500 time series. For validation and testing data, we generate 100 time series for each type of change and evaluate them separately. In the training process, we do not need any label. We only use validation set for hyper parameter tuning.

## 5.3. Evaluation Metric

For quantitative evaluation of CPD performance, we use the following proposed metrics.

- **AUC-ROC** The area-under-the-curve of receiver operating characteristic (AUC-ROC) is a common metric in CPD literature (Li et al., 2015; Liu et al., 2013; Xu et al., 2017; Chang et al., 2019).
- **L1 Distance** The AUC-ROC metric treats each instance independently, but due to delayed prediction, the highest peak of change-point scores could appear after the label. L1 Distance measure the absolute value of difference between the label  $l$  and highest peak  $y$  of the predicted score  $p$ :  $\|y - l\|$ .
- **Triangle Utility** We also consider a hinge-loss-based metric to give percentage score of the predicted highest peak:  $\max(0, 1 - \frac{\|y - l\|}{w})$ , where  $w$  is a window set to 15.

## 5.4. Baselines

We compare our CORD-CPD with the state-of-the-art statistical and deep learning models:

- **ARGP-BODPD** (Saatçi et al., 2010) is Bayesian change-point model that uses auto-regressive Gaussian Process as underlying predictive model.
- **RDR-KCPD** (Liu et al., 2013) uses relative density ratio technique that considers f-divergence as the dissimilarity measure.
- **Mstats-KCPD** (Li et al., 2015) uses kernel maximum mean discrepancy (MMD) as dissimilarity measure on data space.
- **KL-CPD** (Chang et al., 2019) uses deep neural models for kernel learning and generative method to learn pseudo anomaly distribution.
- **LSTNet** (Lai et al., 2018) combines CNN and RNN to extract long- and short-term features for multivariate time series.

## 5.5. Main Results

In Table 1, the first panel represents three statistical baseline model, followed by three state-of-the-art deep learning models. In the bottom panel, we show the ensemble change-point score predicted by CORD-CPD, which significant

improvement over both statistical model and deep learning models on the all the three types of changes.

**CORD-CPD** Among the three types of changes, the score of connection change is lower than the other two, indicating detecting correlation changes is harder than independent changes. Our **Trans<sub>SE</sub>+RNN<sub>TE</sub>** performs the best at detecting the independent changes, while our **GNN<sub>SE</sub>+RNN<sub>TE</sub>** performs the best at detecting the correlation changes. The reason could be that transformers are better at identifying local changes, while RNNs are more stable at combining long term features.

**Statistical Models** For all types of changes, the statistical models are not as competitive as the deep learning models. One explanation is that both **Mstats-KCPD** and **RDR-KCPD** are kernel methods that measures the distribution distance with simple kernel and mean heuristic. The dynamics rule of the physics system could be hard to capture by those methods. Also, the statistical methods have slightly better performance on correlation changes than independent changes. That could be because the once the connection is re-sampled, the trajectories of particles could change much more than the perturbation of speed and velocity features.

**Deep Learning Models** Among the deep learning models, **LSTNet** has better performance on location and speed changes than connection change, and it could be that the CNNs better capture local features and help determine the independent changes. This confirms that GNNs have better inductive bias for learning relations than CNNs and RNNs alone. The kernel based deep learning model **KL-CPD** demonstrates better performance on correlation change than independent change, which is consistent with results of statistical kernel models.

## 5.6. Change-point Type Classification

CORD-CPD separately predicts change-point scores for correlation change and independent change. We show its performance on separating the two reasons of changes, and then perform a change-point type classification experiment.

### 5.6.1. CORRELATION Vs. INDEPENDENT CHANGE

In Table 2, we separately evaluate the scores for correlation change-point (rel) and independent change-point score (ind). Predictions of independent changes are scored high on location and speed change, while predictions of correlation changes are scored high on connection change. This result shows that our system can indeed capture the two types of changes.

**Location&speed** Compared with correlation changes, the independent changes are easier to be separated. The AUC

model	location			speed			connection		
	AUC	DIST	TRI	AUC	DIST	TRI	AUC	DIST	TRI
<b>ARGP-BOCPD</b>	0.5244	22.92	0.0880	0.5231	23.31	0.0660	0.5442	20.86	0.1287
<b>RDR-KCPD</b>	0.5095	22.89	0.0680	0.5279	21.93	0.1093	0.5234	20.51	0.0860
<b>Mstats-KCPD</b>	0.5380	22.59	0.0730	0.5369	22.83	0.0727	0.5508	20.25	0.0833
<b>RNN</b>	0.5413	15.46	0.2567	0.5381	15.26	0.2660	0.5446	12.93	0.3047
<b>LSTNet</b>	0.5817	12.54	0.3487	0.5817	12.50	0.3460	0.5337	15.80	0.2193
<b>KL-CPD</b>	0.5247	19.12	0.1053	0.5378	18.58	0.1352	0.5574	11.63	0.3127
<b>GNN<sub>SE</sub>+RNN<sub>TE</sub></b>	0.9864	0.60	0.9740	0.9700	<b>1.27</b>	<b>0.9320</b>	<b>0.9681</b>	1.57	<b>0.9153</b>
<b>TransSE+RNN<sub>TE</sub></b>	<b>0.9885</b>	<b>0.46</b>	<b>0.9773</b>	<b>0.9755</b>	1.84	0.9080	0.9469	<b>1.44</b>	0.9040
<b>GNN<sub>SE</sub>+Trans<sub>TE</sub></b>	0.9692	1.27	0.9333	0.9609	2.86	0.8473	0.8840	2.33	0.8527

Table 1. We report the AUC, L1 Distance and Triangle Utility for the predicted change-point, CORD-CPD has the best performance on all the change-point types. The models we propose uses different spatial and temporal encoding layers for the encoder.

model	type	location			speed			connection		
		AUC	DIST	TRI	AUC	DIST	TRI	AUC	DIST	TRI
<b>GNN<sub>SE</sub>+RNN<sub>TE</sub></b>	rel	0.5145	14.27	0.3153	0.5590	13.58	0.3553	<b>0.9649</b>	<b>1.40</b>	<b>0.9073</b>
	ind	<b>0.9835</b>	<b>0.62</b>	<b>0.9727</b>	<b>0.9587</b>	<b>1.00</b>	<b>0.9493</b>	0.8093	5.01	0.7320
<b>TransSE+RNN<sub>TE</sub></b>	rel	0.4944	15.67	0.2626	0.5463	13.86	0.3266	<b>0.9755</b>	<b>1.09</b>	<b>0.9273</b>
	ind	<b>0.9859</b>	<b>0.57</b>	<b>0.972</b>	<b>0.9685</b>	<b>1.52</b>	<b>0.9233</b>	0.7774	6.86	0.6460
<b>GNN<sub>SE</sub>+Trans<sub>TE</sub></b>	rel	0.5544	12.06	0.3467	0.5832	10.80	0.4266	<b>0.9098</b>	<b>1.82</b>	<b>0.8787</b>
	ind	<b>0.9855</b>	<b>0.65</b>	<b>0.9693</b>	<b>0.9623</b>	<b>1.69</b>	<b>0.9133</b>	0.7912	4.08	0.7620

Table 2. Our CORD-CPD calculates scores for correlation change-point (rel) and independent change-point (ind). We evaluate them separately on the test data. We observe that predictions of independent changes are scored high on location and speed changes, while predictions of correlation changes are scored high on connection changes.

scores of predictions of location and speed changes are over 0.97, nearly perfectly detects the independent changes. Whereas the AUC scores the connection change are close to 0.5, nearly a random guess. That shows that the encoder doesn't signal correlation change-point for location and speed change, but it gives a strong signal for correlation change-point when spring reconnection happens.

**Connection** CORD-CPD gives similar pattern for the connection change, meaning that it can distinguish the two types of changes for spring reconnections. However, while the AUC scores for correlation are over 0.9, the scores for independent are also around 0.8, unlike what is observed in location & speed. Although a relational change is successfully detected, the recovered time series value is not that accurate. The reason could be that the errors made by encoder is propagated to the decoder, and thus made the expected independent value inaccurate.

#### 5.6.2. CHANGE-POINT TYPE CLASSIFICATION

While our model has robust performance on CPD, it can also distinguish between the correlation changes and independent changes. We use the difference between normalized correlation change-point score  $s_r$  and independent change-

point score  $s_d$  as an indicator of change-point type:

$$\text{Norm}(s_r) - \alpha \text{Norm}(s_d) > \tau$$

where  $\alpha = 0.75$  is our design choice, and  $\tau$  is a threshold separating correlation change and independent change. Moving the value of  $\tau$  controls the type I and type II error, and we use AUC-ROC and AUC-PR metric to show the performance of change-type classification in Table 3.

Model/Metric	AUC-ROC	AUC-PR
<b>GNN<sub>SE</sub>+RNN<sub>TE</sub></b>	0.972	0.962
<b>TransSE+RNN<sub>TE</sub></b>	<b>0.979</b>	<b>0.968</b>
<b>GNN<sub>SE</sub>+Trans<sub>TE</sub></b>	0.916	0.874

Table 3. AUC-ROC and AUC-PR for different  $\tau$  values which controls the type I and type II errors made in change-point type classification

Our best model **TransSE+RNN<sub>TE</sub>** achieves an AUC-ROC of 0.979 and an AUC-PR of 0.968. This indicates that our model has a strong ability to discriminate the two types of change-points. **GNN<sub>SE</sub>+Trans<sub>TE</sub>** has the worst classification performance, which is consistent to the observation in table 2 that it is not good at capturing correlation changes.

### 5.6.3. ABLATION STUDY

We also give an ablation study on the accuracy of change-point type classification. We conduct experiment in two settings, supervised and unsupervised, according to whether the labeled change-point is provided. In the experiments, we set  $\tau = 0$ , results are shown in Table 6.

**Supervised Setting** In real life application, our model can help experts find the cause of a change-point. Assume we are given when a change-point happened, we want to predicted whether it is from a correlation change or independent change.

**Unsupervised Setting** Labeling change-points could be expensive. When a change-point is not provided, we classify the change-point by the predicted highest peak.

**Results** A high accuracy of 98% on identifying the location and speed change demonstrate that our model has high confident predicting the independent changes. For correlation changes, the **TransSE+RNN<sub>TE</sub>** shows the best performance by achieving 93% on supervised setting and 84% on unsupervised setting.

model	location	speed	connection
Supervised			
<b>GNN<sub>SE</sub>+RNN<sub>TE</sub></b>	<b>98%</b>	<b>97%</b>	68%
<b>TransSE+RNN<sub>TE</sub></b>	<b>98%</b>	96%	<b>93%</b>
<b>GNN<sub>SE</sub>+Trans<sub>TE</sub></b>	<b>98%</b>	96%	87%
Unsupervised			
<b>GNN<sub>SE</sub>+RNN<sub>TE</sub></b>	<b>98%</b>	<b>96%</b>	73%
<b>TransSE+RNN<sub>TE</sub></b>	96%	92%	<b>84%</b>
<b>GNN<sub>SE</sub>+Trans<sub>TE</sub></b>	91%	83%	75%

Table 4. We report the accuracy of supervised change type classification vs. the supervised change type classification

model	AUC	DIST	TRI
<b>ARGP-BOCPD</b>	0.5079	24.32	0.1773
<b>RDR-KCPD</b>	0.5633	24.08	0.1933
<b>Mstats-KCPD</b>	0.5112	27.80	0.1480
<b>RNN</b>	0.5540	15.06	0.2393
<b>LSTNet</b>	0.5688	12.14	0.3145
<b>KL-CPD</b>	0.5326	17.18	0.2102
<b>GNN<sub>SE</sub>+RNN<sub>TE</sub></b>	0.7868	7.16	0.7574
<b>TransSE+RNN<sub>TE</sub></b>	0.7903	6.54	0.7750
<b>GNN<sub>SE</sub>+Trans<sub>TE</sub></b>	<b>0.8277</b>	<b>4.20</b>	<b>0.8020</b>

Table 5. We report the performance of our CORD-CPD on a real-world multivariate time series. The variables are sensors and the features includes temperatures and 3-D motions. The change-points are transitions between activities.

## 6. Physical Activity Monitoring Data Set

In addition to our synthetic dataset, we test our model on a real-world dataset called PAMAP2 Physical Activity Monitoring dataset (Reiss & Stricker, 2012). The dataset contains sensor data collected from 9 subjects performing 18 different physical activities, such as walking, cycling, playing soccer. Specifically, the variables we consider are 3 Inertial Measurement Units (IMU) on wrist, chest and ankle respectively, measuring 10 features including temperature, 3D acceleration, gyroscope and magnetometer. Change-points are the transitions between activities.

During transition between activities, independent changes could possibly include the rising of temperature and correlation changes could be the different cooperation patterns between wrist, chest and ankle.

In pre-processing, we down-sample the time-series by 20 and slice them into windows of a fixed length of 100. Each window contains exactly one transition from range [25, 75]. There are totally 184 change-points: 150 are used as training, 14 are used as validation and 20 are used as testing.

The results are shown in 5. Our model achieves the best performance among the 6 statistical and deep learning baselines. We attribute the enhanced performance to the ability of our model to better capture two types of change-points and successfully ensemble them, since in real-world, the cause of change-point could be a mixture of independent change and correlation change.

## 7. Conclusion

In this paper, we study the change point detection problem on multivariate time series data. We focus on detecting two types of change points: the correlation change and independent change. We propose CORD-CPD to capture two types of change-points scores using a correlation encoder and dynamic decoder. The encoder consists of spatial encoding layer, which captures interactions among variables, and a temporal encoding layer, which incorporates time dependent features. We conduct extensive experiments on physical simulation dataset to demonstrate that CORD-CPD can distinguish the two types of change-points, and compare with competitive statistical and deep learning baselines on real-word PAMAP2 dataset to show the enhanced robustness on CPD.

## References

Adams, R. P. and MacKay, D. J. Bayesian online change-point detection. *arXiv preprint arXiv:0710.3742*, 2007.

Barry, D. and Hartigan, J. A. A bayesian analysis for change point problems. *Journal of the American Statistical Association*

ciation, 88(421):309–319, 1993.

Box, G. E., Jenkins, G. M., Reinsel, G. C., and Ljung, G. M. *Time series analysis: forecasting and control*. John Wiley & Sons, 2015.

Chang, W.-C., Li, C.-L., Yang, Y., and Póczos, B. Kernel change-point detection with auxiliary deep generative models. *arXiv preprint arXiv:1901.06077*, 2019.

Cho, K., Van Merriënboer, B., Gulcehre, C., Bahdanau, D., Bougares, F., Schwenk, H., and Bengio, Y. Learning phrase representations using rnn encoder-decoder for statistical machine translation. *arXiv preprint arXiv:1406.1078*, 2014.

Cleland, I., Han, M., Nugent, C., Lee, H., McClean, S., Zhang, S., and Lee, S. Evaluation of prompted annotation of activity data recorded from a smart phone. *Sensors*, 14(9):15861–15879, 2014.

Durbin, J. and Koopman, S. J. *Time series analysis by state space methods*. Oxford university press, 2012.

Ebrahimbadeh, Z., Zheng, M., Karakas, S., and Kleinberg, S. Pyramid recurrent neural networks for multi-scale change-point detection. 2018.

Garnett, R., Osborne, M. A., Reece, S., Rogers, A., and Roberts, S. J. Sequential bayesian prediction in the presence of changepoints and faults. *The Computer Journal*, 53(9):1430–1446, 2010.

Gombay, E., Horváth, L., and Husková, M. Estimators and tests for change in variances. *Statistics & Risk Modeling*, 14(2):145–160, 1996.

Gretton, A., Borgwardt, K. M., Rasch, M. J., Schölkopf, B., and Smola, A. A kernel two-sample test. *Journal of Machine Learning Research*, 13(Mar):723–773, 2012.

Guttenberg, N., Virgo, N., Witkowski, O., Aoki, H., and Kanai, R. Permutation-equivariant neural networks applied to dynamics prediction. *arXiv preprint arXiv:1612.04530*, 2016.

Jang, E., Gu, S., and Poole, B. Categorical reparameterization with gumbel-softmax. *International Conference on Learning Representations (ICLR)*, 2017.

Kawahara, Y., Yairi, T., and Machida, K. Change-point detection in time-series data based on subspace identification. In *Seventh IEEE International Conference on Data Mining (ICDM 2007)*, pp. 559–564. IEEE, 2007.

Khan, H., Marcuse, L., and Yener, B. Deep density ratio estimation for change point detection. *arXiv preprint arXiv:1905.09876*, 2019.

Kim, T. and Choi, J. Reading documents for bayesian online change point detection. In *Proceedings of the 2015 Conference on Empirical Methods in Natural Language Processing*, pp. 1610–1619, 2015.

Kipf, T., Fetaya, E., Wang, K.-C., Welling, M., and Zemel, R. Neural relational inference for interacting systems. In *International Conference on Machine Learning*, pp. 2693–2702, 2018.

Kipf, T. N. and Welling, M. Semi-supervised classification with graph convolutional networks. *arXiv preprint arXiv:1609.02907*, 2016.

Kool, W., Van Hoof, H., and Welling, M. Attention, learn to solve routing problems! *arXiv preprint arXiv:1803.08475*, 2018.

Lai, G., Chang, W.-C., Yang, Y., and Liu, H. Modeling long- and short-term temporal patterns with deep neural networks. In *The 41st International ACM SIGIR Conference on Research & Development in Information Retrieval*, pp. 95–104. ACM, 2018.

Li, S., Xie, Y., Dai, H., and Song, L. M-statistic for kernel change-point detection. In *Advances in Neural Information Processing Systems*, pp. 3366–3374, 2015.

Li, S., Jin, X., Xuan, Y., Zhou, X., Chen, W., Wang, Y.-X., and Yan, X. Enhancing the locality and breaking the memory bottleneck of transformer on time series forecasting. In *Advances in Neural Information Processing Systems*, pp. 5244–5254, 2019.

Li, Y., Meng, C., Shahabi, C., and Liu, Y. Structure-informed graph auto-encoder for relational inference and simulation.

Liu, S., Yamada, M., Collier, N., and Sugiyama, M. Change-point detection in time-series data by relative density-ratio estimation. *Neural Networks*, 43:72–83, 2013.

Moskina, V. and Zhigljavsky, A. Application of the singular spectrum analysis for change-point detection in time series. *Journal of Time Series Analysis*, submitted, 2001.

Reddy, S., Mun, M., Burke, J., Estrin, D., Hansen, M., and Srivastava, M. Using mobile phones to determine transportation modes. *ACM Trans. Sen. Netw.*, 6(2):13:1–13:27, March 2010. ISSN 1550-4859. doi: 10.1145/1689239.1689243. URL <http://doi.acm.org/10.1145/1689239.1689243>.

Reiss, A. and Stricker, D. Introducing a new benchmarked dataset for activity monitoring. In *2012 16th International Symposium on Wearable Computers*, pp. 108–109. IEEE, 2012.

Saatçi, Y., Turner, R. D., and Rasmussen, C. E. Gaussian process change point models. In *ICML*, pp. 927–934, 2010.

Sukhbaatar, S., Fergus, R., et al. Learning multiagent communication with backpropagation. In *Advances in neural information processing systems*, pp. 2244–2252, 2016.

Vaswani, A., Shazeer, N., Parmar, N., Uszkoreit, J., Jones, L., Gomez, A. N., Kaiser, Ł., and Polosukhin, I. Attention is all you need. In *Advances in neural information processing systems*, pp. 5998–6008, 2017.

Xu, K., Hu, W., Leskovec, J., and Jegelka, S. How powerful are graph neural networks? *arXiv preprint arXiv:1810.00826*, 2018.

Xu, K., Li, J., Zhang, M., Du, S. S., Kawarabayashi, K., and Jegelka, S. What can neural networks reason about? *CoRR*, abs/1905.13211, 2019. URL <http://arxiv.org/abs/1905.13211>.

Xu, Z., Kersting, K., and von Ritter, L. Stochastic online anomaly analysis for streaming time series. In *IJCAI*, pp. 3189–3195, 2017.

Xuan, X. and Murphy, K. Modeling changing dependency structure in multivariate time series. In *Proceedings of the 24th international conference on Machine learning*, pp. 1055–1062, 2007.

Yang, Z., Zhao, J., Dhingra, B., He, K., Cohen, W. W., Salakhutdinov, R. R., and LeCun, Y. Glomo: Unsupervised learning of transferable relational graphs. In *Advances in Neural Information Processing Systems*, pp. 8950–8961, 2018.

Yu, R., Zheng, S., Anandkumar, A., and Yue, Y. Long-term forecasting using tensor-train rnns. *Arxiv*, 2017.

Zheng, Y., Liu, L., Wang, L., and Xie, X. Learning transportation mode from raw gps data for geographic applications on the web. In *Proceedings of the 17th International Conference on World Wide Web, WWW '08*, pp. 247–256, New York, NY, USA, 2008. ACM. ISBN 978-1-60558-085-2. doi: 10.1145/1367497.1367532. URL <http://doi.acm.org/10.1145/1367497.1367532>.

Zheng, Y., Chen, Y., Li, Q., Xie, X., and Ma, W.-Y. Understanding transportation modes based on gps data for web applications. *ACM Transaction on the Web*, 4:1–36, January 2010. URL <https://www.microsoft.com/en-us/research/publication/understanding-transportation-modes-based>

## A. Synthetic Data Demo

We plot an example of the synthetic change-point data in Figure 8. We show the trajectories of 5 particles before and after a change-point, where the dashed lines represent the expected trajectory if no change-point happened, and the solid lines are the observed trajectory.

### A.1. Location Change

The location change example is shown in Figure 8(a). In this case, we treat the location as multivariate time series, and we observe a small shift of location at and after the change-point. The gap between the expected value and observed value is maintained during the particle movement, but it may vary due to the complicated interactions between those variables.

### A.2. Velocity Change

The velocity change example is shown in Figure 8(b). Compared with the location change, there is no immediate shift in the time series value observed. The gap between the expected value and the observed value tend to become more obvious over time. This is due to the nature of speed such that a small perturbation can cause large difference in location over long time. In order to detect such kind of changes, a window based comparison (of expected values and observed values) introduced in Section 3 is preferable to using only a single predicted time step.

### A.3. Connection Change

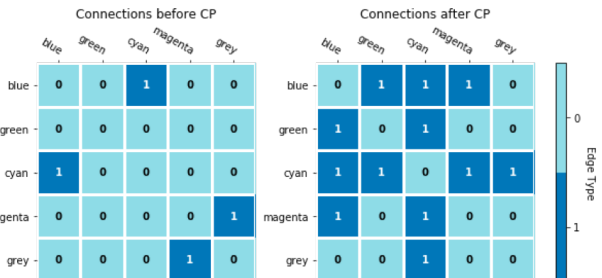


Figure 4. The connections before and after the change-point for the correlation change example.

The connection change example is shown in Figure 8(c). Similar to the velocity change, the difference between the expected value and the observed value becomes more obvious over time. The Figure 4 shows the underlying spring connections before and after the change-point. In particular, the *green* particle was not connected with any other particles before the change-point, and it was connected with *blue* and *cyan* particles after the change-point. This altered the trajec-

tory of the *green* particle from a straight line to curved path. Detecting the spring re-connections change-points requires the modelling of dynamic correlations in multivariate time series, as our model did.

## B. Further Analysis on Synthetic Experiments

In this section, we further describe our model training, baselines, and some other metrics on the synthetic dataset.

### B.1. Implementation Detail

We perform a grid search for hyperparameters of the following values: the learning rate  $l_r$  in  $\{0.001, 0.005, 0.01, 0.05\}$ , the hidden dimension size  $d$  for the time series feature embeddings in  $\{64, 128, 256\}$ , and the number of levels of GNN or spatial transformer in  $\{2, 3, 4\}$ . We finally selected  $l_r = 0.001$  using Adam optimizer,  $d = 64$  for transformers and  $d = 256$  for GNN. The level of GNN or spatial transformer is set as 2, which is sufficient for our experiments. We used batch size of 32 for temporal and spatial transformers and batch size of 128 for GNN.

We report the results for three encoder models: **GNN<sub>SE</sub>+RNN<sub>TE</sub>**, **Trans<sub>SE</sub>+RNN<sub>TE</sub>** and **GNN<sub>SE</sub>+Trans<sub>TE</sub>**. Using both temporal and spatial transformer modules was hard to optimize and resulted in degraded performance, so we didn't include it as our model.

### B.2. Correlation prediction Accuracy

Since the ground truth connections of springs (**A**) are known in the synthetic dataset, we can calculate the accuracy of learnt correlation ( $\hat{\mathbf{A}}$ ). The accuracy  $p_{acc}$  is calculated by

$$p_{acc} = \frac{1}{T \times N \times (N-1)} \sum_{t=1, i < j}^{t \leq T} \mathbb{1}_{\{\hat{\mathbf{S}}_{i,j}^t = \mathbf{A}_{i,j}^t\}}$$

$$\hat{\mathbf{S}}_{i,j}^t = \begin{cases} 1, & \text{if } \hat{\mathbf{A}}_{i,j}^t \geq 0.5 \\ 0, & \text{otherwise} \end{cases}$$

Where  $\hat{\mathbf{S}}$  is the sampled categorical relation.  $T$  is the number of time step and  $N$  is the number of variables. For every pair of variables  $i, j$ , the function  $\mathbb{1}$  is an indicator function which outputs 1 if  $\hat{\mathbf{S}}_{i,j}^t = \mathbf{A}_{i,j}^t$ , and 0 otherwise.

model	location	speed	connection
<b>GNN<sub>SE</sub>+RNN<sub>TE</sub></b>	96.07%	96.04%	90.45%
<b>Trans<sub>SE</sub>+RNN<sub>TE</sub></b>	<b>97.79%</b>	97.36%	<b>93.11%</b>
<b>GNN<sub>SE</sub>+Trans<sub>TE</sub></b>	97.49%	<b>97.47%</b>	92.53%

Table 6. The accuracy of predicted connections compared with ground truth connections in synthetic dataset.

We observe that spatial and temporal transformers achieve better performance in the accuracy metrics, with **Trans<sub>SE</sub>+RNN<sub>TE</sub>** the being best on location and connection change, and nearly competitive as **GNN<sub>SE</sub>+Trans<sub>TE</sub>** on velocity changes. This result is consistent in the CPD task, such that **Trans<sub>SE</sub>+RNN<sub>TE</sub>** has the best score for separated predictions of independent changes and correlation changes.

### B.3. Correlation vs. Independent Change

In the experiment, our model separately predicts the correlation change-point score by the correlation encoder, and the independent change-point score by the dynamics decoder. We also report the results when the two scores are separately evaluated. In Figure 7, we plot the two types of scores predicted by our model in the three types of changes, and the ground truth change-point label as the red dashed line.

We observe that for location and velocity changes, the independent scores are peaked at the labeled change-point; For connection changes, the correlation scores are peaked at the labeled change-point. We conclude that model has the ability to separate the two types of change-points.

### B.4. Change-point Type Classification

In the change-type classification experiment in Section 5, we propose to evaluate our model in both supervised setting and unsupervised setting. In the supervised setting, the time step of change-point is provided, and our goal is to predict the whether the change-point is resulted from an independent change or a correlation change. In the unsupervised setting, the time step of change-point not given, and we use the predicted change-point by our ensemble model instead.

Our model separately predicts  $s_r$ , the correlation change-point score, and  $s_d$ , the independent change-point score. The change-point type is determined by  $\text{Norm}(s_r) - \alpha \text{Norm}(s_d)$ , such that

$$\text{Norm}(s_r) - \alpha \text{Norm}(s_d) \begin{cases} \geq \tau, & \text{correlation change} \\ < \tau, & \text{independent change} \end{cases}$$

Where  $\alpha$  is a hyperparameter and  $\tau$  is a threshold. Norm is the mean-std normalization function.

In our study, we set  $\tau = 0$  and visualize (in Figure 5) how  $\alpha$  value affects the change-point type classification accuracy. The model we choose is **GNN<sub>SE</sub>+Trans<sub>TE</sub>**. We observe that if  $\alpha$  is small, the correlation change-point score dominates, and connection changes are more accurately predicted. When  $\alpha$  is large, the independent change-point score dominates, and the location and velocity changes are more accurately predicted. As a trade off between the two, we choose  $\alpha = 0.75$  in the experiment section.

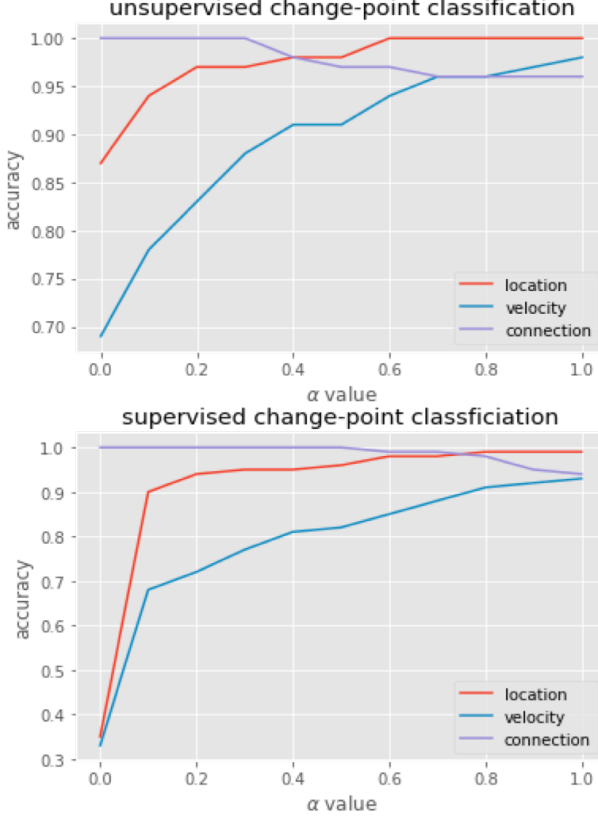


Figure 5.  $\alpha$  value vs. the change-point type classification accuracy.  $\alpha$  is in range  $[0, 1]$ .

### B.5. Discussion on CPD

In the experiments, we use three metrics: *AUC-ROC*, *DIST* and *TRI*. The *AUC-ROC* score was widely used in previous literatures (Li et al., 2015; Liu et al., 2013; Xu et al., 2017; Chang et al., 2019), but *DIST* and *TRI* are what we proposed in this paper. The reason is that *AUC-ROC* treats each instance independently, but time-series data has a strong locality dependence. We do observe cases where the peak of the prediction is close to but not aligned with the labels, as shown in Figure 6.

We observe that our model has the best performance in all the three metrics. For statistical and other deep learning baselines, we observe that they have similar *AUC-ROC*, but the statistical models are worse at *DIST* and *TRI* metrics. The reason is that statistical model concatenates a window sampled from training data at the start and end of each test case, to avoid the cold-start problem. However, this may lead the algorithm to give higher scores at the start or end of the test cases, resulting a larger gap from the labeled change-point.

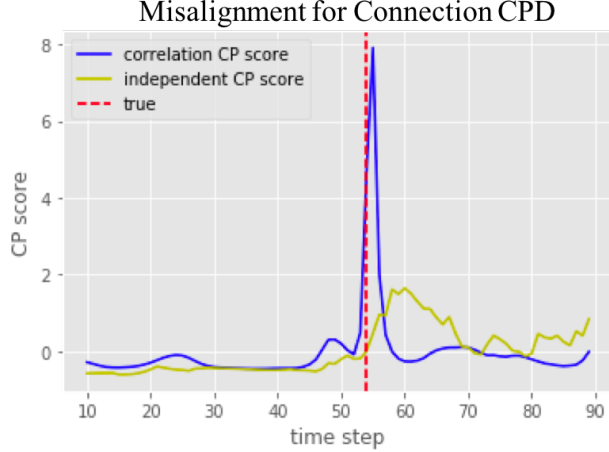


Figure 6. The peak of prediction is not aligned with the label, but very close due to a 1-step delay.

### C. Robust CPD on Real Data

In Table 7, we report the performance of CORD-CPD on the real-world PAMAP2 dataset. The multivariate time series includes 3 variables and 10 features. The variables are sensors on wrist, chest and ankle, and the features are temperature, 3D acceleration, gyroscope and magnetometer. The change-points are transitions between activities, such as walking, cycling, playing soccer.

In the real-world scenario, the change-points are often resulted from a mixture of correlation change and independent change. We show the evaluated scores for the predicted correlation changes and independent changes of each model in Table 7. We have two observations: 1) Each model capture similar trends for correlation changes and independent changes. There are more independent changes than correlation changes involved. 2) The ensemble of two reasons of change-points further boosts the performance, as the true reason of the change-point could include both of them.

### D. Desiderata and Related Work

In this section, we conclude our project with the settings of our model and related work to emphasize our contribution and difference from the previous methods.

#### D.1. Settings

**Unsupervised** In real life, training labels for change-points are hard to obtain, so we want our model to learn the patterns in an unsupervised settings.

**Multivariate Time Series** Multivariate time series is ubiquitous in our life. We focus on change-point detection

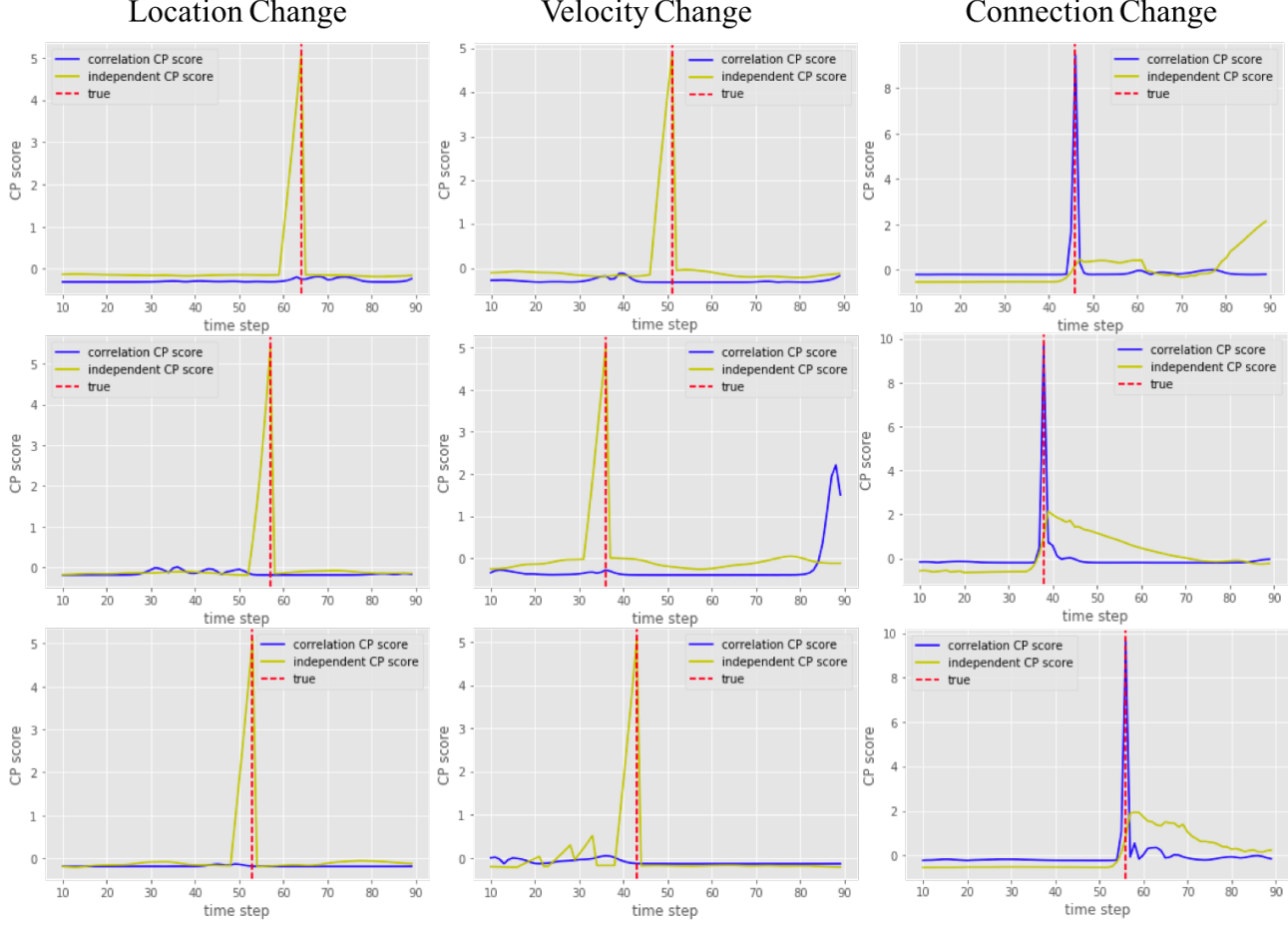


Figure 7. We show the correlation change-point score and the independent change-point score in the three types of change-points. The ground-truth change-point is labeled as red dashed line.

model	type	AUC	DIST	TRI
<b>GNN<sub>SE</sub>+RNN<sub>TE</sub></b>	rel	0.6882	10.40	0.5972
	ind	0.7850	7.73	0.7088
	ens	0.7868	7.16	0.7574
<b>Trans<sub>SE</sub>+RNN<sub>TE</sub></b>	rel	0.6538	13.95	0.4118
	ind	0.7722	7.73	0.7360
	ens	0.7903	6.54	0.7750
<b>GNN<sub>SE</sub>+Trans<sub>TE</sub></b>	rel	0.6715	15.04	0.4013
	ind	0.7787	8.10	0.7102
	ens	<b>0.8277</b>	<b>4.20</b>	<b>0.8020</b>

Table 7. The performance of our CORD-CPD on a real-world PAMAP2 dataset for CPD. We include the scores of independent changes and correlation changes as well.

by modelling multivariate time series.

**Interpretability** Previous work in CPD literature mostly focuses on detecting change-points instead of providing explanations to them. We give an attempt to reason the causes behind change-points as correlation changes and independent changes.

**Neural Architecture** We give our effort to explore the application of deep learning models in CPD.

**Graph Neural Networks** Previous neural models mostly rely on CNNs and RNNs to extract local and long term dependencies (Lai et al., 2018). For relational learning, GNNs may have better inductive bias and we incorporate it into our encoder and decoder.

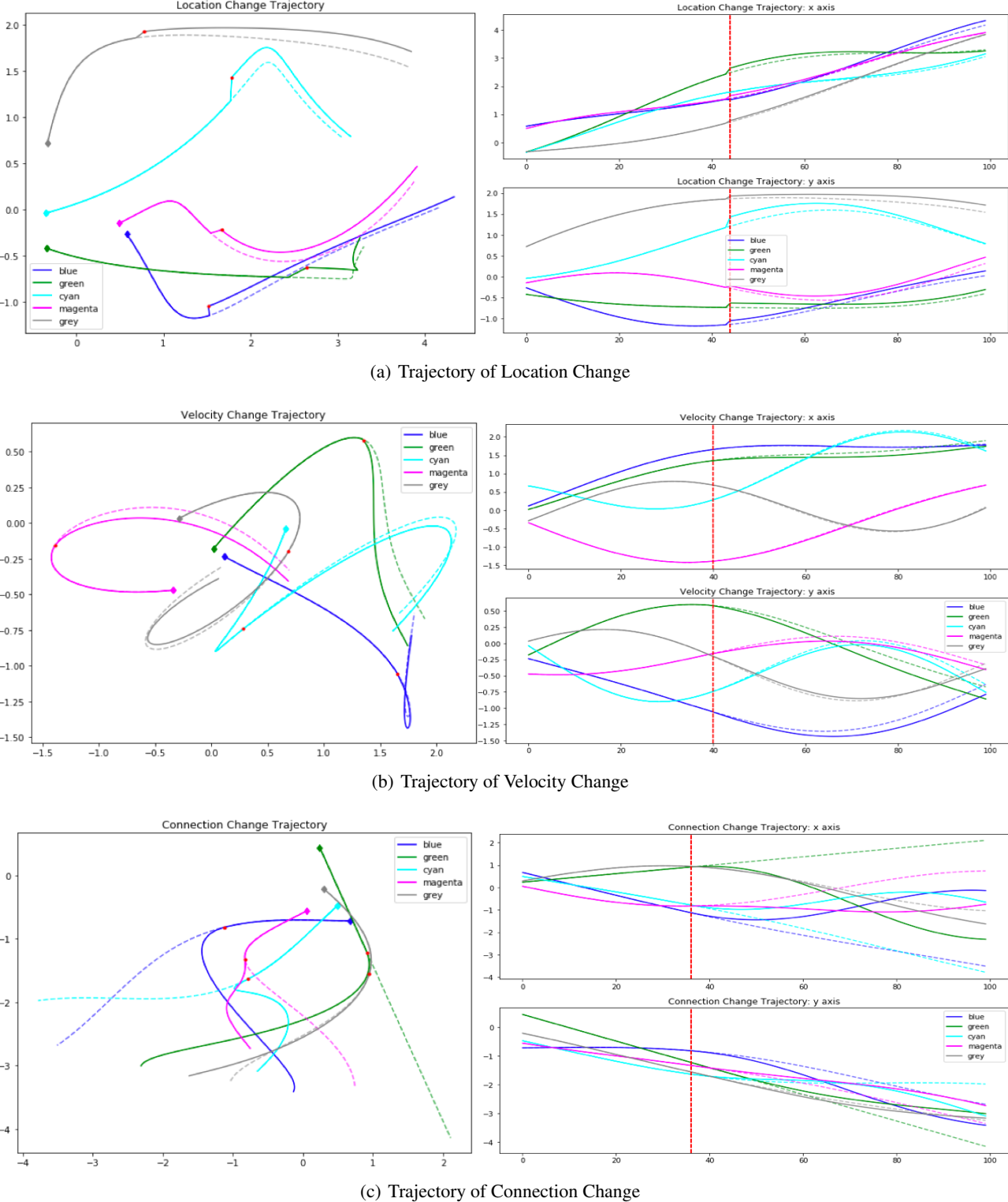


Figure 8. The three figures show the trajectories of different types of change-points of 5 particles (in 5 colors) connected by underlying springs. The figures on the left show the 2-D trajectories of the particles, and the figures on the right show the x and y axis of the trajectories separately. The dashed lines represent the expected trajectory if no change-point happened, and the solid lines are the actual observed trajectory.

## D.2. More on Related Work

### D.2.1. TIME SERIES FORECASTING

Time series forecasting aims at predicting future time steps based on historical observations on time series signals, with a wide range of applications including forecasting new trends or generating alert for potential hazardous events. Traditional time series forecasting models uses State Space Models (SSMs) (Durbin & Koopman, 2012) and Autoregressive (AR) models (Box et al., 2015). Recently, deep learning models uses CNN, RNN and Transformer models to extract features automatically and predict the future steps (Lai et al., 2018; Li et al., 2019; Yu et al., 2017).

Time series forecasting can be applied to CPD by comparing the expected future steps with the observed value. In our work, we use the forecasting models as baselines to calculate the change-point scores.

### D.2.2. GRAPH NEURAL NETWORKS

Graph Neural Networks have attracted considerable amount of attention in deep learning community. As graph is a natural way to represent underlying interactions between objects, learning a relational graph in a data-driven approach is interesting. Recently, GloMo (Yang et al., 2018) proved that the relations between units learned by GNN from text and image in one dataset can be generalized to other datasets in transfer learning setting. Neural relational inference (Kipf et al., 2018) extracts non-changing relations from time series data, and structure-informed graph auto-encoder (Li et al.) incorporated prior knowledge as regularization to disentangle different relations from time series.

Besides the success of graph networks in applications, researchers are devoted to a theoretical understanding of the capacity of GNN. Graph Neural Networks recursively gather messages from local neighborhood and combine them by an aggregation scheme to form new node features. This recursive aggregation scheme grants GNN the power to be better aligned with relation learning tasks (Xu et al., 2019), and different ways of combining messages results in different capacity in those tasks (Xu et al., 2018). In our work, we study how to use GNN networks to extract dynamic correlation from time-series data and its applications to CPD.

### D.2.3. CHANGE-POINT DETECTION

In supervised setting, various methods have been applied to model the phases in time series, including decision tree (Zheng et al., 2010), Bayesian net (Zheng et al., 2008), support vector machine (Reddy et al., 2010), Gaussian mixture model (Cleland et al., 2014) etc. Recently, deep learning models using wave-net style architecture for supervised CPD (Ebrahimzadeh et al., 2018). Supervised methods such as decision trees could possibly give explanations on

change-points, but the labels are usually hard to obtain in large quantities.

In the unsupervised setting, most statistical CPD models are based on statistical inference, or hypothesis tests. Bayesian CPD models (Barry & Hartigan, 1993; Xuan & Murphy, 2007) computes the probability of change-points using the Bayesian framework. BOCPD algorithms (Adams & MacKay, 2007; Garnett et al., 2010; Saatçi et al., 2010; Kim & Choi, 2015) detect change-points by sequentially considering the correlated intervals between them. Recent deep learning models improves the state-of-the-art statistical methods by approximating density ratio (Khan et al., 2019), or learning kernel functions (Chang et al., 2019) using neural networks.

Our work belongs to the unsupervised deep learning CPD methods, but we propose a novel encoder-decoder architecture to learn correlation changes and independent changes, and ensemble them for final predictions.